SCIENTIFIC REPORTS

OPEN

SUBJECT AREAS:
MATERIALS SCIENCE
APPLIED PHYSICS
NANOTECHNOLOGY
SURFACE CHEMISTRY

Received
18 April 2012

Accepted
29 May 2012

Published
15 June 2012

Correspondence and requests for materials should be addressed to Z.Z. (zzhan@mail.sic.ac.cn)

# A micro-nano porous oxide hybrid for efficient oxygen reduction in reduced-temperature solid oxide fuel cells

Da Han, Xuejiao Liu, Fanrong Zeng, Jiqin Qian, Tianzhi Wu & Zhongliang Zhan

CAS Key Laboratory of Materials for Energy Conversion, Shanghai Institute of Ceramics, Chinese Academy of Sciences (SICCAS), 1295 Dingxi Road, Shanghai 200050, P. R. China.

**Tremendous efforts to develop high-efficiency reduced-temperature ($\leq 600^{\circ}C$) solid oxide fuel cells are motivated by their potentials for reduced materials cost, less engineering challenge, and better performance durability. A key obstacle to such fuel cells arises from sluggish oxygen reduction reaction kinetics on the cathodes. Here we reported that an oxide hybrid, featuring a nanoporous $Sm_{0.5}Sr_{0.5}CoO_{3-\delta}$ (SSC) catalyst coating bonded onto the internal surface of a high-porosity $La_{0.9}Sr_{0.1}Ga_{0.8}Mg_{0.2}O_{3-\delta}$ (LSGM) backbone, exhibited superior catalytic activity for oxygen reduction reactions and thereby yielded low interfacial resistances in air, *e.g.*, 0.021 $\Omega$ cm$^2$ at 650$^{\circ}$C and 0.043 $\Omega$ cm$^2$ at 600$^{\circ}$C. We further demonstrated that such a micro-nano porous hybrid, adopted as the cathode in a thin LSGM electrolyte fuel cell, produced impressive power densities of 2.02 W cm$^{-2}$ at 650$^{\circ}$C and 1.46 W cm$^{-2}$ at 600$^{\circ}$C when operated on humidified hydrogen fuel and air oxidant.**

Solid oxide fuel cells (SOFCs) are attractive for clean efficient conversion of fuels into electricity[1]. SOFCs also show compelling potentials for efficient production of fuels from renewable electricity[2,3] and electricity storage[4]. Although some SOFC systems are available for residential and business power generation, the high operating temperature of 700–1000$^{\circ}$C leads to prohibitive system costs, high degradation rates and slow startup times, seriously impeding the widespread practical implementation of the technology. An effective approach to address the above issues is to lower the operating temperature down to $T \leq 600^{\circ}C$[5], where the fuel cell efficiency is nevertheless largely determined by the activation of oxygen reduction reactions (ORR) on the cathodes[6]. As a consequence, the last decade has witnessed a significant amount of efforts aimed at identifying new cathode materials and/or microstructures that would exhibit outstanding ORR catalytic activity and therefore allow low polarization resistances[7–12].

The standard cathode material for SOFCs with the state-of-the-art yttria-stabilized zirconia (YSZ) electrolytes is a composite of Sr-doped $LaMnO_3$ (LSM) and YSZ[1,13]. Restriction of oxygen reduction reaction to the contiguous contact of electronic, ionic and gas phases or the so-called triple phase boundaries (TPB)[12], due to the pure electronic conducting nature of LSM, necessitates an operating temperature in excess of 750$^{\circ}$C in order to achieve reasonably high electrochemical activity and thus yield relatively low polarization resistances, *e.g.*, $R_P < 0.2\ \Omega$ cm$^2$ at 800$^{\circ}$C. Reducing temperature down to 600$^{\circ}$C produced undesirably large $R_P$ values ($\approx 2\ \Omega$ cm$^2$)[14]. On the other hand, mixed-conducting oxides exhibit simultaneous transport of electrons and oxide ions, allow oxygen reduction reaction to proceed on the whole electrode surface, and thereby enable low $R_P$ values at reduced temperatures[12,13]. Shao and Haile showed that $Ba_{0.5}Sr_{0.5}Co_{0.8}Fe_{0.2}O_{3-\delta}$ (BSCF) demonstrated fast kinetics for surface oxygen exchange and produced low $R_P$ values of 0.055–0.071 $\Omega$ cm$^2$ at 600$^{\circ}$C or 0.2 $\Omega$ cm$^2$ at 550$^{\circ}$C[8]. Recently, Zhou *et al* reported that the $R_P$ values were larger for the pristine BSCF cathode, *e.g.*, 0.16 $\Omega$ cm$^2$ at 600$^{\circ}$C or 0.45 $\Omega$ cm$^2$ at 550$^{\circ}$C, while coating the BSCF backbones with a thin shell of A-site deficient BSCF to form a heterostructured cathode can increase the surface oxygen exchange rate by 220–330%, and can thereby reduce the $R_P$ value down to 0.06 $\Omega$ cm$^2$ at 600$^{\circ}$C or 0.15 $\Omega$ cm$^2$ at 550$^{\circ}$C[15]. Despite these extensive efforts, developing oxygen electrode catalysts to efficiently catalyze oxygen reduction reaction over the reduced-temperature regime of 500–600$^{\circ}$C remains a significant challenge. Here we report a micro-nano porous oxide hybrid consisting of a nanoporous SSC catalyst coating supported on the internal surfaces of a high-porosity LSGM backbone that

exhibited superior ORR catalytic activity and thereby yielded low polarization resistances at reduced temperatures.

## Results

**Fabrication and structure of the SSC/LSGM hybrid.** The micro-nano oxide hybrid was based upon porous LSGM backbones (Figure S1), as synthesized by the ceramic tape casting method. LSGM was used as the supporting component due to its high oxide ionic conductivity and negligibly low electronic conductivity at reduced temperatures[16]. Use of starch as the fugitive material in the tape casting formulation resulted in a uniform porous microstructure with an average pore size of ≈ 3 μm and an estimated porosity of ≈ 55%. Then, a thin layer of SSC was coated on the internal surfaces of the porous LSGM backbones using the aqueous nitrate solution impregnation, followed by calcinations at 850°C. SSC was chosen as the catalyst due to its high oxide ion diffusivity, fast oxygen surface exchange kinetics and high electronic conductivity[17]. A single impregnation/calcination cycle yielded a SSC loading $V_{SSC}$ of 1.5% in the porous LSGM backbone, and the SEM micrograph of the resulting coating indicated that a substantial fraction of the SSC catalyst particles appeared physically isolated from each other, and the average particle size was ≈ 70 nm (Figure S2).

Note that these SSC infiltrates play dual roles in the porous LSGM backbones: catalyzing oxygen reduction reaction and collecting the electrical current. Well-connected coatings are mandatory for effective implementation of both functions, and can be readily attained at higher catalyst loadings via multiple impregnation/calcination cycles. Fig. 1a shows an SEM micrograph of the SSC/LSGM hybrid at $V_{SSC}$ = 12.9% that exhibited substantially improved phase connectivity. In the meanwhile, increasing the number of impregnation/calcination cycles increased the catalyst coating thickness on the pore walls as well. For example, the SSC particles increased to ≈ 100 nm at $V_{SSC}$ = 12.9%, as shown in Fig. 1b. Such an increase in the catalyst particle size can be ascribed to repeated calcination cycles that inevitably caused agglomeration and coarsening of these nanoparticulates. Nevertheless, the cost-effective and manufacturing-scalable chemical solution impregnation technology enabled the formation of nanoporous and well intra-connected SSC electrocatalyst coatings on the internal surfaces of the porous LSGM backbones.

**Electrochemical characteristics of the SSC/LSGM hybrid.** An effective measure of the catalytic activity of the fuel cell cathode for oxygen reduction reactions is the area specific polarization resistance ($R_P$), which can be obtained from the electrochemical impedance spectroscopy (EIS) measurements on symmetric cathode fuel cells, *e.g.,* SSC-LSGM hybrid/LSGM electrolyte/SSC-LSGM hybrid. Such symmetric cells were based upon an LSGM tri-layer: 300 μm and 60 μm thick porous layers separated by a 15 μm thick dense layer. The active SSC component was added to the porous LSGM backbones by wet impregnation and subsequent calcinations, as described above. The impedance data were collected under a uniform atmosphere of ambient air.

Fig. 2a shows a representative Nyquist plot of the EIS data in air at 600°C from a symmetric fuel cell at $V_{SSC}$ = 12.9%, where the high frequency real-axis intercept is primarily associated with the cell ohmic loss ($R_o$) and the difference between the high and low frequency real-axis intercept corresponds to the $R_P$ value. Notably, the polarization resistance at 600°C was 0.043 Ω cm² for the micro-nano porous SSC/LSGM hybrid at $V_{SSC}$ = 12.9%. For comparison, the state-of-the-art micron-scale SOFC cathodes have larger $R_p$ values at comparable temperatures, *e.g.*, > 2 Ω cm² for LSM-YSZ[14], 0.5 Ω cm² for random $Sm_{0.5}Sr_{0.5}CoO_{3-\delta}$-$La_{0.8}Sr_{0.2}Ga_{0.8}Mg_{0.15}Co_{0.05}O_{3-\delta}$ (SSC-LSGMC) composites[18], 0.12 Ω cm² for Pd-promoted SSC-LSGMC composites[18], 0.055-0.071 Ω cm² for BSCF reported by Shao and Haile[8] or 0.06 Ω cm² for heterostructured BSCF by Zhou *et al*[15].

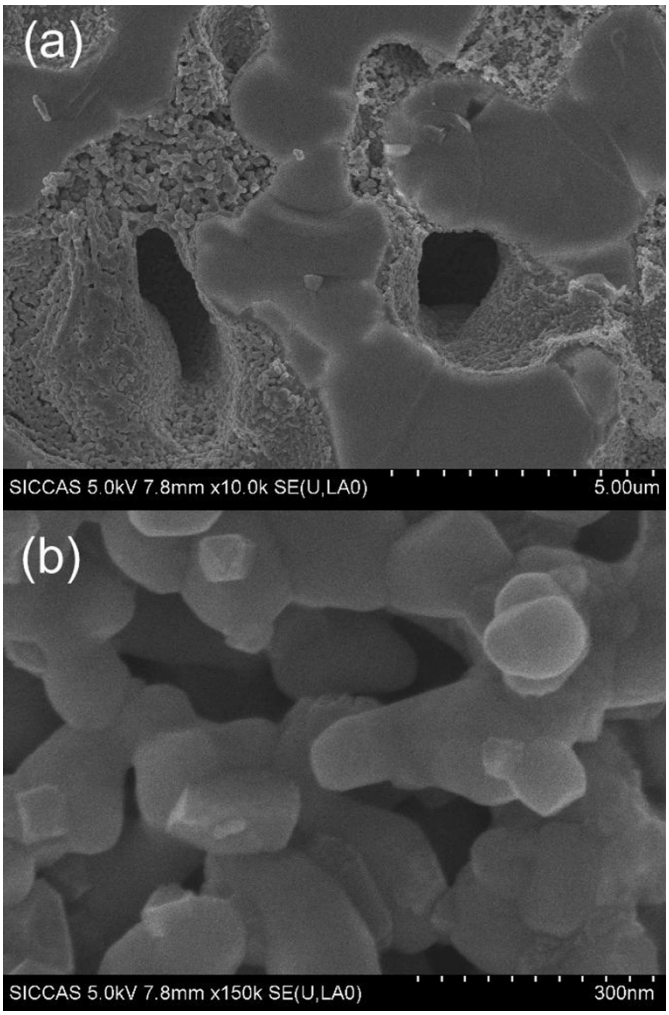


**Figure 1 | Cross-sectional SEM micrographs showing the structure of the micro-nano porous SSC/LSGM hybrid.** (a) A low magnification survey of the hybrid. (b) A high magnification view of the SSC catalyst.

Fig. 2b summarizes the $R_o$ and $R_P$ values at varied SSC loadings. Both values increased slightly with $V_{SSC}$ decreasing from 12.9% to 8.6%, but then increased rapidly with further decrease in $V_{SSC}$. For example, the $R_P$ value increased substantially to 0.26 Ω cm² at $V_{SSC}$ = 4.3%. The increase in the ohmic resistance and the cathode polarization resistance with decreasing $V_{SSC}$ can be explained by the decreasing SSC phase connectivity (Figure S2), which decreased the electronic conductivity and reduced the fraction of total SSC surface area that is electrochemically active, *i.e.*, where electrons are available from the external circuit via electrically contiguous SSC–SSC particle contacts. Additionally, the total SSC surface area became smaller with decreasing $V_{SSC}$, resulting in a more pronounced increase in the $R_P$ value. For the SSC-LSGM hybrid at $V_{SSC}$ = 12.9%, the measured ohmic resistance was ≈ 0.093 Ω cm² at 600°C. Based upon the measured oxide ion conductivity of 0.027 S cm$^{-1}$ at 600°C, the expected resistance for a 15 μm-thick LSGM electrolyte is ≈ 0.056 Ω cm². The additional 0.04 Ω cm² may arise from current collection losses or elsewhere in the testing setup given that the $V_{SSC}$ = 12.9% SSC-LSGM hybrid showed an electrical conductivity of ≈ 10 S cm$^{-1}$ at 600°C and thereby yielded negligible ohmic contribution (0.0036 Ω cm² at 0.36 mm thick SSC-LSGM layers for the present symmetric cells).

Durability is a potential concern for the present micro-nano porous SSC/LSGM hybrid since nano-particle coarsening can reduce the surface area available for surface oxygen exchange. Prior report has

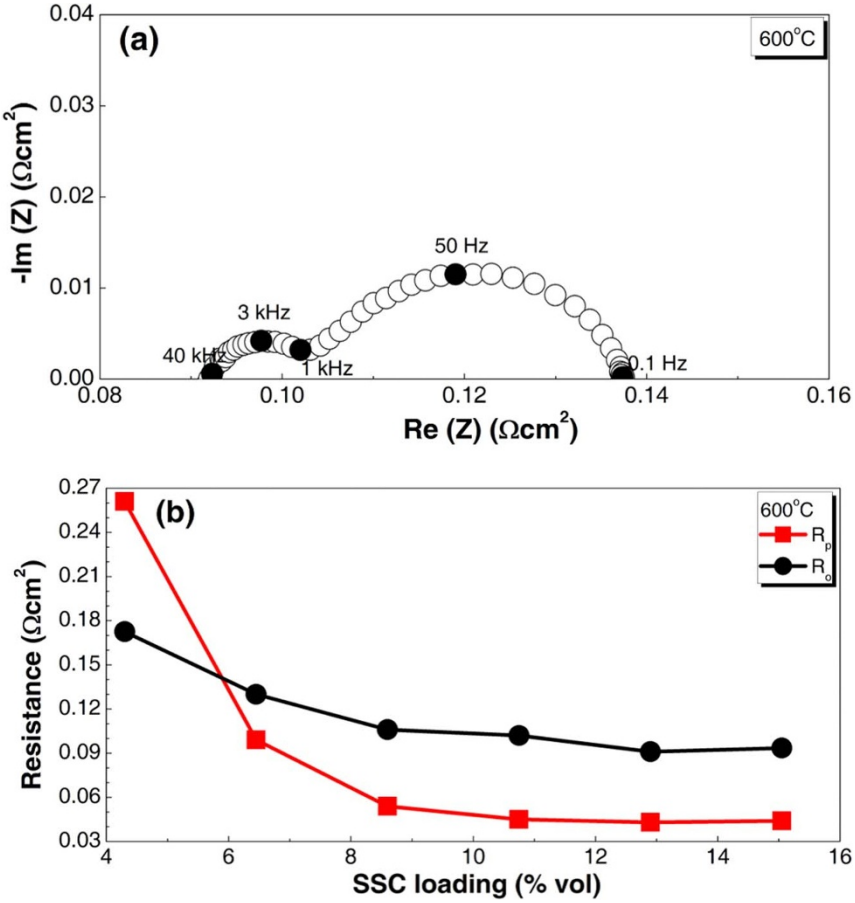


**Figure 2 | Impedance measurements on symmetric cathode fuel cells in ambient air.** (a) Representative impedance spectra measured at 600°C for the SSC/LSGM hybrid at $V_{SSC}$ = 12.9%. (b) The cathode polarization resistance (Rp) and the ohmic resistance (Ro), derived from the impedance data, plotted versus the SSC loading.

shown that the time-dependence of the cathode polarization resistance followed a power law model based upon surface diffusion limited coarsening, and that the $R_P$ value became increasingly stable with decreasing the aging temperature from 850°C to 650°C[19]. Indeed, a few tests on the present SSC/LSGM hybrid indicted that the cathode polarization resistance remained almost unchanged, *e.g.*, ≈ 0.135 Ω cm², over a duration of 100 h at 550°C. Nevertheless, more extended testing is required for better evaluation of the performance durability.

**Fuel cell performance.** The electrochemical properties of the micro-nano porous SSC/LSGM hybrid were also examined on an anode-supported fuel cell (Figure S3). The LSGM electrolyte was typically 15 μm thick. The anode consisted of 7.2 vol% Ni in the porous LSGM (Figure S4), and these nano-scale Ni particles could yield a high TPB density to produce small polarization resistances, *e.g.*, 0.026 Ω cm² in 97% $H_2$ – 3% $H_2O$ at 650°C[6]. Fig. 3a shows the cell voltages and power densities as a function of current densities for such a fuel cell, operating on 97% $H_2$ – 3% $H_2O$ and ambient air at 500–650°C. Note that the fuel utilization was typically low, *e.g.*, < 6% at 0.7 V, such that the influence of the gas flow geometry on the fuel cell performance was excluded. The cell exhibited high open circuit voltage (OCV) values between 1.09 V and 1.11 V and provided maximum power densities of 2.02, 1.46, 0.91 and 0.47 W cm$^{-2}$ at 650, 600, 550 and 500°C, respectively. The Nyquist plot of the impedance data, as shown in Fig. 3b, showed that the overall area specific resistance (ASR) was as small as ≈ 0.17 Ω cm² at 650°C and open circuits for the fuel cell. The present results compare favorably with prior reduced-temperature fuel cells. Yan *et al* reported maximum power densities of 1.95 W cm$^{-2}$ at 600°C for the pulsed laser deposited LSGM/doped ceria bi-layer electrolyte fuel cells[20,21]. However, such high power densities were obtained with pure oxygen as the oxidant that could substantially increase the cathode performance[6]. Shao and Haile reported maximum power densities of 1 W cm$^{-2}$ at 600°C for thin doped-ceria electrolyte fuel cells[8]. Nonetheless, the electronic conduction in doped-ceria resulted in reduced OCV values and fuel efficiency losses[8]. Recently, anode-supported $Er_{0.8}Bi_{1.2}O_3$/doped-ceria bi-layer electrolyte fuel cells were fabricated by combining high temperature ceramic processing and low temperature pulsed laser deposition, and demonstrated maximum power densities of 1.95 W cm$^{-2}$ at 650°C[22]. While the 4 μm-thick $Er_{0.8}Bi_{1.2}O_3$ layer has no appreciable electronic conductivity in air, a much thicker layer of doped ceria (10 μm thick in ref. 22) was used on the fuel side to prevent decomposition of the $Er_{0.8}Bi_{1.2}O_3$ layer. Despite the synergistic structure, the resulting open circuit voltage of 0.77 V was still much lower than the theoretically expected value of 1.13 V. Increasing the thickness ratio of doped-ceria/$Er_{0.8}Bi_{1.2}O_3$ to 48μm/4μm could yield a high OCV value of 0.88 V at 650°C[5], but in the meanwhile produce much larger ohmic resistances that might limit the fuel cell performance.

## Discussions

Oxygen reduction on the fuel cell cathode is complicated and consists of consecutive steps including oxygen molecule diffusion within the pores, dissociative adsorption of oxygen molecules, surface diffusion and ionization of adsorbed oxygen atom, oxide ion conduction in the bulk cathode and oxide ion transfer at the cathode/electrolyte

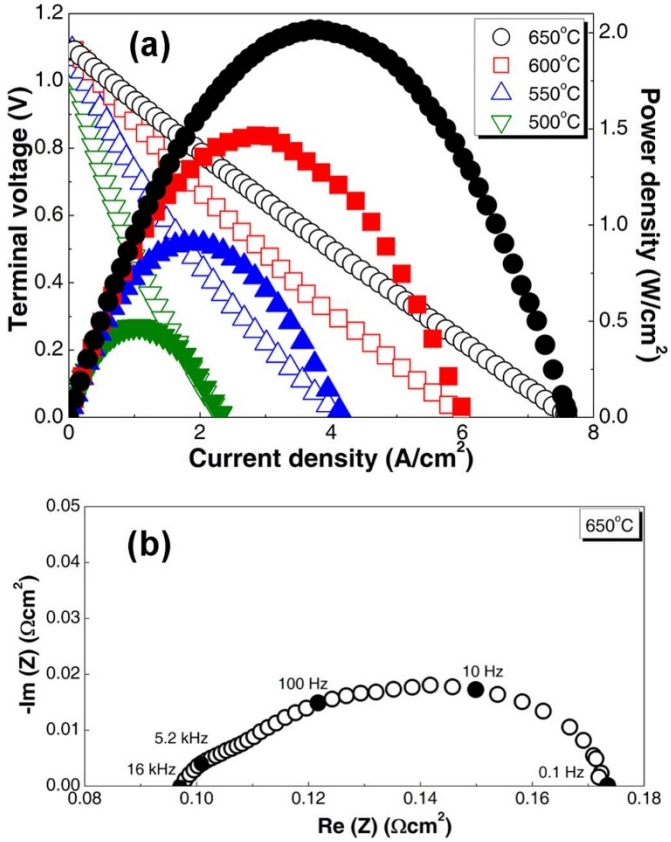


**Figure 3 | Characteristics of an anode-supported, thin LSGM electrolyte fuel cell with electrode loadings $V_{Ni}$ = 7.2% and $V_{SSC}$ = 12.9% measured in 97% $H_2$ – 3% $H_2O$ fuels and ambient air oxidants.** (a) Plots of voltage and power density versus current density at 500–650°C. (b) Representative impedance spectra measured at 650°C and open circuits.

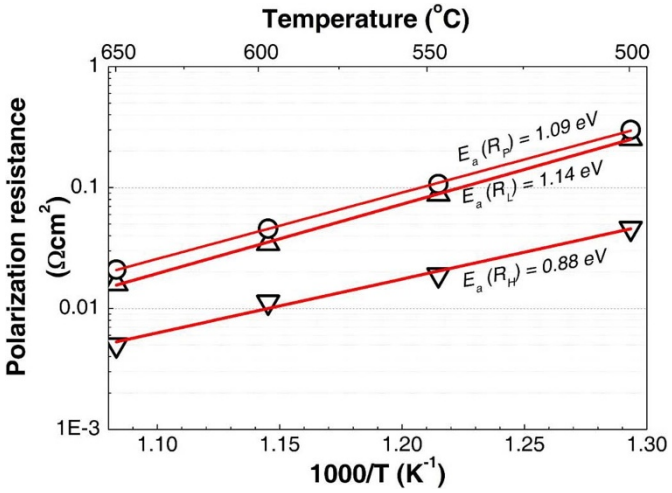


**Figure 4 | Impedance analysis on the symmetric cathode fuel cells in ambient air.** The total cathode polarization resistance, the high-frequency and low-frequency polarization resistances for the SSC/LSGM hybrid at $V_{SSC}$ = 12.9%, derived from the impedance data, plotted versus inverse temperature.

interface. The Nyquist plot in Fig. 2a consists of a small high-frequency arc ($R_h$) at ≈ 3 kHz and a large low-frequency arc ($R_l$) at ≈ 50 Hz, which can be attributed to the charge transfer reaction on the SSC/LSGM and oxygen surface exchange on the SSC/gas interfaces[23]. Note that the oxide ion conduction through the bulk SSC coating in the micro-nano porous hybrid made little contribution to the low-frequency diffusion resistances since the characteristic thickness ($L_c$) for SSC, defined as the ratio of oxygen self-diffusion coefficient $D^*$ ($cm^2\ s^{-1}$) to the surface exchange coefficient $k$ ($cm\ s^{-1}$), *i.e.*, $L_c = D^*/k$, is on the order of 100 μm which is three orders of magnitude larger than the thickness of the SSC coatings in the present work (0.1 μm)[17]. The $R_h$ and $R_l$ values at varied temperatures are estimated from the Nyquist plots, as summarized in Fig. 4 together with the total $R_P$ values. The overall cathode polarization resistance increased from 0.021 Ω $cm^2$ at 650°C to 0.3 Ω $cm^2$ at 500°C. The $R_l$ value is 3–5 times larger than $R_h$, suggesting that surface oxygen exchange is the rate-limiting step in the electrochemical oxygen reduction reactions. The activation energies for the charge transfer reaction, surface oxygen exchange and the overall oxygen reduction are 0.88, 1.14 and 1.09 eV, respectively. The Simple Infiltrated Microstructure Polarization Loss Estimation (SIMPLE) model[24], derived from the Tanner, Fung and Virkar (TFV) model[25], was proposed by Nicholas and Barnett to correlate the cathode polarization resistance to the SSC surface area and the intrinsic SSC surface resistance. The validity of the model was further confirmed by the cathode surface oxygen exchange resistance predictions that were within 15% of the experimentally measured $R_l$ values at all temperatures (Table S1). The impressively low polarization resistance for the present SSC/LSGM hybrid as the fuel cell cathode can be ascribed to the nano-scale SSC particles and the resulting high surface area available for oxygen reduction reactions.

The oxide ionic conductivity of the supporting component and the electrolyte critically influences the electrochemical and catalytic behavior of the micro-nano porous hybrids. For comparison, another hybrid of SSC/YSZ (Figure S5) was fabricated based upon a porous | dense | porous YSZ tri-layer structure that had almost the same pore structure as the LSGM counterpart. YSZ was chosen since it is also a pure oxide ionic conductor, but has much smaller conductivities (*e.g.*, 0.002 S/cm at 600°C) than the present LSGM support. Impedance measurement showed substantially larger $R_P$ values for the SSC/YSZ hybrid. For example, the polarization resistance at 650°C was 0.40 Ω $cm^2$ for the SSC/YSZ hybrid at $V_{SSC}$ = 13%, which is approximately 20 times the value for the above SSC/LSGM hybrid at a comparable SSC loading (Figure S6). Note that the low calcination temperature of 850°C was critical to minimize the formation of an insulating $SrZrO_3$ from the interaction between the SSC infiltrates and the YSZ backbones that might produce undesirably large $R_P$ values[26]. This is further supported by the low $R_P$ value of 0.04 Ω $cm^2$ at 800°C for the SSC/YSZ hybrid (Figure S6). Given that both hybrids had very similar nanoporous SSC coatings, it is reasonable to assume that the surface oxygen exchange kinetics was essentially the same. The large difference in the $R_P$ value at 650°C can thereby be attributed to very different oxide ionic diffusivities in the supporting component that are closely related to the charge transfer reaction occurring on the SSC/backbone interfaces. As a matter of fact, the activation energy for the overall oxygen reduction over the SSC/YSZ hybrid was 1.30 eV, indicating that charge transfer reaction might be the rate-limiting step. Therefore, the combined features in the SSC/LSGM hybrid – high oxide ionic conductivity of the LSGM support and rapid surface oxygen exchange of the nanoporous SSC coating – enabled the outstanding oxygen reduction kinetics and the resulting low polarization resistance values.

To illustrate the importance of the pore structure of the support in promoting oxygen reduction kinetics, an alternative pore former with very different morphology was used in the tape casting formulation for the porous LSGM layer. The resulting porous | dense | porous LSGM tri-layer structure had approximately the same porosity of 55% but with a larger mean pore size of 10 μm (Figure S7). Despite the fact that oxygen molecular transport became facilitated within larger pores, impedance measurement showed an approximately 2–4 times increase in the cathode polarization resistance for

the resulting 10 μm SSC/LSGM hybrid when compared with the above 3 μm SSC/LSGM hybrid at comparable SSC loadings. In particular, the $R_P$ values in air at $V_{SSC}$ =13% were 0.08 Ω cm$^2$ at 650°C and 0.26 Ω cm$^2$ at 550°C (Figure S8). These results demonstrate that an optimal pore structure of the support, in addition to the high oxide ionic conductivity, is also mandatory for fast oxygen reduction kinetics on the micro-nano porous hybrid.

In summary, we have fabricated a novel hybrid of SSC/LSGM by coating a thin nanoporous SSC layer onto the internal surface of a micron-porous LSGM backbone. We have also demonstrated that the pore structure and the oxide ionic conductivity of the LSGM support, in addition to the nano-scale structure of the SSC coating, are critically important for obtaining rapid oxygen reduction kinetics in the application as the reduced-temperature solid oxide fuel cell cathode. The area specific resistance for oxygen reduction can be as low as 0.021 and 0.043 Ω cm$^2$ in air at 650 and 600°C, respectively.

## Methods

The porous | dense | porous LSGM tri-layer structure was produced by laminating three tape-cast ceramic green tapes, with 40 wt% rice starch filler used as the fugitive material for the two porous layers. The LSGM powders (5 m$^2$g$^{-1}$) were supplied by Praxair Specialty Ceramics. The laminated green tapes were co-fired at 1450°C to produce the final ceramic structures. SSC was added into the porous LSGM backbones by impregnating an aqueous nitrate solution of 2 M containing $Sm(NO_3)_3{\cdot}6H_2O$, $Sr(NO_3)_2$ and $Co(NO_3)_2{\cdot}6H_2O$ in appropriate ratios into the porous LSGM backbones, followed by calcinations at 850°C for 4 hours. These nitrates were 99% pure and purchased from Sinopharm Chemical Reagent. The X-Ray diffraction patterns confirmed that the catalyst consisted predominantly of perovskite structure SSC with minor impurity phases $Co_3O_4$, $SmCoO_3$, and $SrCoO_3$[24]. Note that multiple impregnation/firing cycles were usually used in order to introduce a sufficient amount of SSC into the LSGM backbones. The quantity of the deposited SSC catalysts was estimated by the weight difference before and after each impregnation/firing cycle. For comparison, the SSC-YSZ hybrids were prepared in the same manner as the SSC-LSGM hybrids. The YSZ powders (7 m$^2$g$^{-1}$) were purchased from Tosoh Corporation.

The electrochemical properties of the SSC-LSGM hybrid were assessed on both symmetric cells and anode-supported cells. For the symmetric cells, SSC was impregnated into both porous layers. For the anode-supported cells, the 60 μm thick porous LSGM layers were impregnated with SSC, while the 300 μm thick porous LSGM substrates were impregnated with a 4 M aqueous nickel nitrate solution followed by calcinations in air at 700°C for 30 minutes that would produce a thin layer of NiO on the internal surfaces of the porous backbones. Silver ink was painted on the electrode surface as the current collector, and silver wires were used as the current leads. The active cathode area was 0.28 cm$^2$.

All impedance data were obtained using an IM6 Electrochemical Workstation (ZAHNER, Germany) with a frequency range from 0.1 Hz to 100 kHz and an ac perturbation of 20 mV. Ambient air was used for the measurement of the cathode polarization resistance in the symmetric cells. The anode supported fuel cell was tested at temperatures from 500°C to 650°C with the cathode exposed to ambient air and the anode to humidified (3% $H_2O$) hydrogen at a flow rate of 100 mL/min. The cell structure was examined after testing using scanning electron microscopy (SEM) in a Hitachi S-4800-II microscope.


1. Minh, N. Q. Ceramic Fuel-Cells. *J. Am. Ceram. Soc.* **76**, 563–588 (1993).
2. Hauch, A., Ebbesen, S. D., Jensen, S. H. & Mogensen, M. Highly efficient high temperature electrolysis. *J. Mater. Chem.* **18**, 2331–2340 (2008).
3. Mogensen, M., Jensen, S. H., Hauch, A., Chorkendorff, I. & Jacobsen, T. Reversible Solid Oxide Cells. *Ceram. Eng. Sci. Proc.* **28**, 91–101 (2008).
4. Bierschenk, D. M., Wilson, J. R. & Barnett, S. A. High efficiency electrical energy storage using a methane–oxygen solid oxide cell. *Energy & Environmental Sci.* **4**, 944–951 (2011).
5. Wachsman, E. D. & Lee, K. T. Lowering the temperature of solid oxide fuel cells. *Science* **334**, 935–939 (2011).
6. Zhan, Z. L., Bierschenk, D. M., Cronin, J. S. & Barnett, S. A. A reduced temperature solid oxide fuel cell with nanostructured anodes. *Energy & Environmental Sci.* **4**, 3951–3954 (2011).
7. Shao, Z. P. Cathode Materials for Solid Oxide Fuel Cells Towards Operating at Intermediate-to-Low Temperature Range. *Prog. Chem.* **23**, 418–429 (2011).
8. Shao, Z. P. & Haile, S. M. A high-performance cathode for the next generation of solid-oxide fuel cells. *Nature* **431**, 170–173 (2004).
9. Kim, Y. N. & Manthiram, A. Layered $LnBaCo_{2-x}Cu_xO_{5+\delta}$ ($0 \le x \le 1.0$) Perovskite Cathodes for Intermediate-Temperature Solid Oxide Fuel Cells. *J. Electrochem. Soc.* **158**, B276–B282 (2011).
10. Sacanell, J., Leyva, A. G., Bellino, M. G. & Lamas, D. G. Nanotubes of rare earth cobalt oxides for cathodes of intermediate-temperature solid oxide fuel cells. *J Power Sources* **195**, 1786–1792 (2010).
11. Jiang, Z. Y., Xia, C. R. & Chen, F. L. Nano-structured composite cathodes for intermediate-temperature solid oxide fuel cells via an infiltration/impregnation technique. *Electrochim. Acta.* **55**, 3595–3605 (2010).
12. Sun, C. W., Hui, R. & Roller, J. Cathode materials for solid oxide fuel cells: a review. *J. Solid State Electr.* **14**, 1125–1144 (2010).
13. Jacobson, A. J. Materials for Solid Oxide Fuel Cells. *Chem. Mater.* **22**, 660–674 (2010).
14. Zhao, L., Ye, X. F. & Zhan, Z. L. High-performance cathode-supported solid oxide fuel cells with copper cermet anodes. *J. Power Sources* **196**, 6201–6204 (2011).
15. Zhou, W., Liang, F., Shao, Z., Chen, J. & Zhu, Z. Heterostructured electrode with concentration gradient shell for highly efficient oxygen reduction at low temperature. *Sci. Rep.* **1**, 155 (2011).
16. Huang, K. Q., Tichy, R. & Goodenough, J. B. Superior perovskite oxide-ion conductor; strontium- and magnesium-doped $LaGaO_3$: III, Performance tests of single ceramic fuel cells. *J. Am. Ceram. Soc.* **81**, 2581–2585 (1998).
17. Fullarton, I. C. *et al.* Study of Oxygen Ion Transport in Acceptor Doped Samarium Cobalt Oxide. *Ionics* **1**, 51–58 (1995).
18. Wang, S. Z. & Zhong, H. High performance Pd promoted $Sm_{0.5}Sr_{0.5}CoO_3$-$La_{0.8}Sr_{0.2}Ga_{0.8}Mg_{0.15}Co_{0.05}O_{3-\delta}$ composite cathodes for intermediate temperature solid oxide fuel cells. *J. Power Sources* **165**, 58–64 (2007).
19. Shah, M., Voorhees, P. W. & Barnett, S. A. Time-dependent performance changes in LSCF-infiltrated SOFC cathodes: The role of nano-particle coarsening. *Solid State Ionics* **187**, 64–67 (2011).
20. Yan, J., Matsumoto, H., Akbay, T., Yamada, T. & Ishihara, T. Preparation of $LaGaO_3$-based perovskite oxide film by a pulsed-laser ablation method and application as a solid oxide fuel cell electrolyte. *J. Power Sources* **157**, 714–719 (2006).
21. Yan, J. W., Matsumoto, H., Enoki, M. & Ishihara, T. High-power SOFC using $La_{0.9}Sr_{0.1}Ga_{0.8}Mg_{0.2}O_{3-\delta}$/$Ce_{0.8}Sm_{0.2}O_{2-\delta}$ composite film. *Electrochem. Solid-State Lett.* **8**, A389–A391 (2005).
22. Ahn, J. S. *et al.* High-performance bilayered electrolyte intermediate temperature solid oxide fuel cells. *Electrochem. Commun.* **11**, 1504–1507 (2009).
23. Adler, S. B., Chen, X. Y. & Wilson, J. R. Mechanisms and rate laws for oxygen exchange on mixed-conducting oxide surfaces. *J. Catal.* **245**, 91–109 (2007).
24. Nicholas, J. D. & Barnett, S. A. Measurements and Modeling of $Sm_{0.5}Sr_{0.5}CoO_{3-x}$-$Ce_{0.9}Gd_{0.1}O_{1.95}$ SOFC Cathodes Produced Using Infiltrate Solution Additives. *J. Electrochem. Soc.* **157**, B536–B541 (2010).
25. Tanner, C. W., Fung, K. Z. & Virkar, A. V. The effect of porous composite electrode structure on solid oxide fuel cell performance .1. Theoretical analysis. *J. Electrochem. Soc.* **144**, 21–30 (1997).
26. Huang, Y. Y., Ahn, K., Vohs, J. M. & Gorte, R. J. Characterization of Sr-doped $LaCoO_3$-YSZ composites prepared by impregnation methods. *J. Electrochem. Soc.* **151**, A1592–A1597 (2004).


## Acknowledgments

The authors gratefully acknowledge the financial support of the National Basic Research Program of China under contract No. 2012CB215400, the National Science Foundation of China under contract No. 51072219, Science and Technology Commission of Shanghai Municipality under contract No. 09JC1415200 and 11PJ1410300, the 100 Talents Program of Chinese Academy of Sciences, Chinese Academy of Sciences visiting professorship for senior international scientists under grant No. 2010T1G09.

## Author contributions

Z.Z. planed the experiments and wrote the paper. D.H., X.L., F.Z., J.Q. and T.W. carried out the experiments.

## Additional information

**Supplementary information** accompanies this paper at http://www.nature.com/scientificreports

**Competing financial interests:** The authors declare no competing financial interests.



**How to cite this article:** Da Han *et al.* A micro-nano porous oxide hybrid for efficient oxygen reduction in reduced-temperature solid oxide fuel cells. *Sci. Rep.* **2**, 462; DOI:10.1038/srep00462 (2012).